

## Satellite Estimates and Shipboard Observations of Downward Radiative Fluxes at the Ocean Surface

G. GUO\* AND J. A. COAKLEY JR.

*College of Oceanic and Atmospheric Sciences, Oregon State University, Corvallis, Oregon*

(Manuscript received 9 February 2007, in final form 10 July 2007)

### ABSTRACT

Clouds and the Earth's Radiant Energy System (CERES) uses a suite of instruments on the *Terra* and *Aqua* satellites combined with analyzed weather data and information on surface conditions to estimate surface radiative fluxes. CERES estimates for the *Terra* satellite were compared with measurements of the surface radiative fluxes collected with the research vessels (RVs) *Wecoma* and *Thomas G. Thompson* radiometers for cruises off the Oregon coast undertaken during 2000–03. To assess the shipboard measurements, the radiometer observations were analyzed to identify cloud-free conditions characterized by ~1–2 h of relatively stable radiative fluxes. Fluxes for the cloud-free conditions were compared with those calculated using profiles of temperature and humidity from analyzed meteorological fields for the times and locations of the measurements and broadband radiative transfer models. For summertime conditions along the Oregon coast, and assuming a marine aerosol having 0.55- $\mu\text{m}$  optical depth of 0.05, modeled and observed values of the shortwave flux agreed to within 1%–2%. Similar comparisons for the downward cloud-free longwave flux were within 1%–3%. This agreement also held for the CERES surface radiative flux estimates with CERES cloud-free fields of view for ocean scenes within 50 km of the ship being compared with 30-min averages of the shipboard measurements centered on the times of the *Terra* overpass. Using the CERES observations to identify cloud-free conditions for the *Wecoma* revealed that in some cases the shipboard measurements of the shortwave flux varied erratically. Criteria were adopted to avoid such behavior, yielding periods in which the surface radiative fluxes were reasonably stable for a range of cloud-free and cloudy conditions. With the criteria applied, the absolute magnitude of the mean differences between the shipboard measurements and the CERES estimates for the downward shortwave flux were within 2%, with RMS differences less than 6% within each month of CERES–shipboard matchups. The absolute magnitude of the mean differences for the downward longwave flux was less than 2%, with RMS differences less than 5%.

### 1. Introduction

The National Aeronautics and Space Administration's (NASA) Clouds and Earth Radiant Energy System (CERES) has, as one of its goals, estimating surface radiative fluxes (Wielicki et al. 1996). Estimates from CERES rely on a mix of broadband radiances, which are obtained from the CERES radiometers on the *Terra* and *Aqua* satellites; high-spatial-resolution

multispectral imagery, obtained from the Moderate Resolution Imaging Spectroradiometer (MODIS); analyzed meteorological fields; aerosol properties derived from MODIS observations and assimilated in an aerosol transport model; and radiative transfer modeling (Charlock et al. 2005). Satellite estimates of surface fluxes are known to have shortcomings. Errors in the downward shortwave flux arise primarily from the absorption of sunlight by aerosols, and those in the downward longwave flux arise primarily from the lack of information on cloud properties, particularly their lower boundaries (Charlock and Alberta 1996). Clearly, the satellite estimates require assessment through comparison with collocated surface measurements that span the range of possible atmospheric conditions. Such comparisons are underway using mostly land- and island-based surface stations (Charlock et al. 2005). The comparisons serve to quantify the accuracy

---

\* Current affiliation: I. M. System Group, Inc., Rockville, Maryland.

---

Corresponding author address: J. A. Coakley Jr., College of Oceanic and Atmospheric Sciences, 104 COAS Admin. Building, Oregon State University, Corvallis, OR 97331-5503.  
E-mail: coakley@coas.oregonstate.edu

of the satellite inferences and thus provide a means of assessing the quality of surface radiative energy budgets constructed from the inferences. For example, in the tropical eastern Pacific, Cronin et al. (2006) found that the radiative fluxes derived from the International Satellite Cloud Climatology Project (ISCCP) observations (Zhang et al. 1995) were sufficiently representative when compared with similar fluxes derived from an array of buoys that the satellite-derived products could be used to assess the surface radiative fluxes calculated in weather forecast and analysis schemes. For vast regions of the ocean, however, like the northeastern Pacific, there are no reliable surface-based observations of the radiative fluxes against which to assess the performance of the satellite inferences.

For many years, shipboard pyranometers and pyrgeometers have been routinely deployed for measuring surface radiative fluxes, but the observations are often considered to be of poor quality and are rarely used. While the radiometers themselves are capable of 1%–2% calibration accuracies (Hosom et al. 1995; Fairall et al. 1998), biases arise from the harsh environment, which leads to coatings on radiometer domes (Medovaya et al. 2002) and tilts from winds and currents. In addition, rocking by sea swell can cause appreciable biases (Katsaros and DeVault 1986; MacWhorter and Weller 1991). Also, the radiometer measurements can suffer from “shadowing” of the fields of view by parts of the ship. The goals of this study are to 1) assess the quality of shipboard pyranometer and pyrgeometer observations collected during operations of the research vessel *Wecoma* off the coast of Oregon and 2) if the assessment indicates that the shipboard data are sufficiently accurate to constrain the satellite-based observations, then to compare the shipboard measurements with simultaneous CERES estimates of the fluxes. While most of the observations analyzed for this study were from the *Wecoma*, operated by Oregon State University’s College of Oceanic and Atmospheric Sciences, some were from the *Thomas G. Thompson*, operated by the National Oceanic and Atmospheric Administration. The *Thompson* data came from a period of joint operations with the *Wecoma* off the Oregon coast.

As others have done (Fairall et al. 1998; Medovaya et al. 2002; Cronin et al. 2006), the strategy for assessing the usefulness of the shipboard observations is to begin with observations under cloud-free conditions. Cloud-free conditions offer the best opportunity for understanding the performance of the shipboard radiometers through comparison with the results of radiative transfer models. Cloud-free conditions entail temporally stable surface radiative fluxes and in the northeastern Pacific, these periods are often accompanied by rela-

tively low humidities and, depending on location and time of year, low aerosol burdens. Radiative transfer models have been demonstrated to predict the surface fluxes under such conditions to within a few percent, close to the accuracies of the shipboard radiometers (Cess et al. 1996; Zender et al. 1997; Jing and Cess 1998; Fairall et al. 1998).

Here the shipboard observations were examined first to assess their quality and second to use the observations in assessing the performance of the CERES estimates of the surface radiative fluxes. Procedures were developed in which the temporal variability of the downward shortwave and longwave fluxes were used to identify cloud-free conditions. Cloud-free observations were then compared with radiative transfer model estimates of the downward fluxes. As the comparisons proved successful, within the limits of error for both the calibration of the radiometers and similar experiences with radiative transfer calculations (Fairall et al. 1998; Medovaya et al. 2002), the cloud-free estimates were then compared with CERES estimates of the downward fluxes. These comparisons also showed excellent agreement. A search of the CERES observations for all cloud-free conditions collocated with the *Wecoma* observations, however, revealed that some of the cloud-free observations were missed. In fact, in some cases, the shipboard pyranometer appeared to exhibit unexplained erratic behavior for conditions that were, based on the satellite observations, free of clouds. New rules were developed to identify possible erratic behavior in the shipboard pyranometer data. These procedures are ad hoc, but provide reasonable precautions for obtaining surface observations with which to compare satellite-derived estimates under a wide range of observing conditions. CERES estimates of the surface radiative fluxes were then compared with the shipboard observations for all-sky conditions. Not surprisingly, applying the screening criteria to remove what appeared to be erratic behavior of the pyranometer substantially improved the agreement between the shipboard measurements and satellite estimates.

## 2. Data

Most of the shipboard pyranometer and pyrgeometer data used in this study came from the *Wecoma*. Approximately three weeks of data came from the *Thomas G. Thompson* during a period when the ships were undertaking a coordinated study off the coast of Oregon. On the *Wecoma*, the pyranometer is an Eppley Precision Spectral Pyranometer and the pyrgeometer is an Eppley Precision Infrared Radiometer. The instruments are mounted on top of the winch house in a

location that allows largely unobstructed views of the sky. This location was a compromise between the needs for the unobstructed views and for keeping the instruments clean and operating during cruises. For the observations used in this study, the radiometers were cleaned, often as much as twice daily, sea state and duties of the technical personnel permitting. Both instruments were connected to amplifiers and analog-to-digital converters mounted just below the instruments through short (0.5 m) shielded cables. The instruments were sent to Eppley each year for calibration. The Eppley calibration data were used to convert the instrument voltages to radiative fluxes. The longwave fluxes were obtained following Eppley's prescription using separate measurements for the case and detector temperatures. The fluxes used for this study were 1-min averages. No corrections were made for differences between the dome and case temperatures of the pyrgeometer (e.g., Fairall et al. 1998), nighttime offsets of the shortwave flux (Cess et al. 2000), effects due to shadowing by the ship's superstructure, and effects that might have resulted from the motion of the ship.

As will be discussed in the next section, pyranometer and pyrgeometer measurements of the downward radiative fluxes identified as being associated with cloud-free conditions were assessed through comparison with the fluxes calculated using detailed radiative transfer models. The profiles of temperature and humidity as well as the surface temperature and surface humidity used in these calculations were obtained from National Centers for Environmental Prediction (NCEP; Kistler et al. 2001) analyzed fields for times that bracketed the overpass of *Terra*, nominally 1100 LST. In addition, the effects of a marine aerosol, described by Hess et al. (1998), were included in the calculation of the fluxes. The marine aerosol is composed of relatively large particles that absorb little sunlight. The discrete ordinate method (Stamnes et al. 1988) in an eight-stream mode was used to calculate the shortwave radiative flux. Gaseous absorption for the shortwave was taken from what is now referred to as the NASA Langley version of the Fu-Liou code (Fu and Liou 1992; Rose and Charlock 2002; Charlock et al. 2005). Shortwave fluxes using this code were within 1%–2% of those calculated using the gaseous absorption model adopted by Coakley et al. (2002). Longwave fluxes were calculated using the Langley version of the Fu-Liou code.

Collocated CERES clouds and radiative swath (CRS) estimates of the shortwave and longwave fluxes were compared with the shipboard measurements and, for cloud-free conditions, the results of the radiative

transfer calculation. The CRS data provide fluxes for individual CERES fields of view that are approximately 20 km across at nadir. The CRS contains several estimates of the radiative fluxes. First a flux is calculated using temperature and humidity profiles derived from the NASA Goddard Earth Observing System (GEOS) Data Assimilation System, version 4 (GEOS4) assimilation of meteorological data, cloud properties derived from MODIS observations (Minnis et al. 2003), and aerosol properties derived from a combination of aerosol optical depths retrieved from MODIS (Remer et al. 2005; Ignatov et al. 2005) and assimilated using the National Center for Atmospheric Research Model for Atmospheric Transport and Chemistry (MATCH). Second, a constrained flux is calculated by adjusting, depending on scene type, aerosol properties, water vapor burdens, and cloud properties within their ranges of expected uncertainties until the radiative flux calculated for the top of the atmosphere matches the CERES estimate derived from a combination of scene type and anisotropic factors (Loeb et al. 2005). The surface fluxes are then calculated using the adjusted cloud, aerosol, and moisture burdens (Charlock et al. 2005). Along with these calculated fluxes, two additional estimates, referred to as models A and B, are offered in the CERES CRS data stream for both shortwave and longwave fluxes. These fluxes are derived from a combination of model calculations and regressions. The A models are based on Li et al. (1993) for the shortwave flux and Inamdar and Ramanaathan (1997) for the longwave flux. The B models, referred to as the Langley Parameterized Shortwave and Longwave Algorithms, are described by Gupta et al. (2004).

### 3. Assessment of shipboard radiometers

The first step in assessing the performance of the shipboard radiometers was to seek observations under cloud-free conditions. As was noted earlier, under cloud-free conditions reasonably accurate estimates of the downward shortwave and longwave radiative fluxes can be calculated. As long as the radiatively active composition is reasonably characterized, the broadband fluxes can be obtained to within 2%–3%, comparable to the best accuracies anticipated for the shipboard flux measurements.

Cloud-free conditions are characterized by long periods (1–2 h) over which the downward shortwave and longwave fluxes vary little. Lines of sight from the surface to the horizon, assuming low-level clouds at 1 km, span a region with radius of order 100 km. Conditions at sea, however, are rarely so cloud free. A clearing

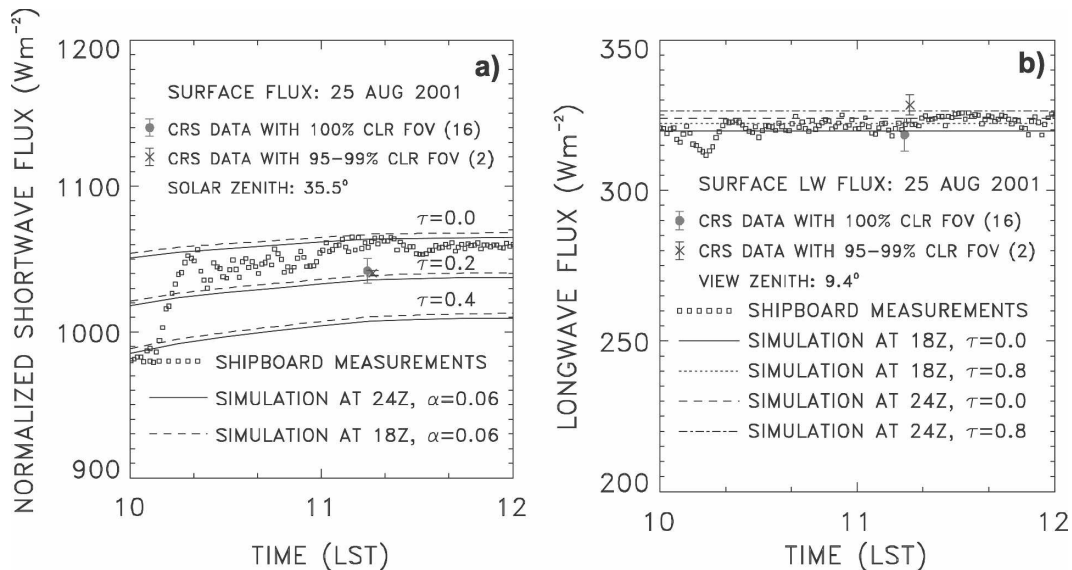


FIG. 1. Downward normalized (a) shortwave and (b) longwave radiative flux 1-min averages (open symbols) measured by the *Wecoma's* radiometers on 25 Aug 2001. At the time of the observations the *Wecoma* was off the coast of Oregon at  $44.6^{\circ}N$ ,  $124.5^{\circ}W$ . The time is LST for the *Wecoma*. Also shown are calculated downward normalized shortwave and longwave radiative fluxes based on the temperatures and humidities at the location of the ship in the 1800 and 2400 UTC NCEP analyses and different values of the  $0.55\text{-}\mu m$  optical depth  $\tau$  for a marine aerosol. CERES CRS constrained estimates of the downward fluxes are also shown for the time of the *Terra* overpass. The estimates are based on 16 cloud-free CERES fields of view (closed circle) and 2 fields of view with 95%–99% cloud cover (cross) within 50 km of the *Wecoma* at the time of the overpass. The error bars give the standard deviation of the CERES CRS estimates. The zenith angles are the average solar zenith and satellite zenith (view zenith) angles for the CERES fields of view used in the comparisons.

with radius of order 10 km would be suggested if low-level clouds at an altitude of 1 km were observed on the horizon with an elevation angle of  $5^{\circ}$ . Ship motion and winds, even as small as  $3\text{ m s}^{-1}$ , would bring such clouds over the radiometers within the course of an hour or so, giving rise to considerable variability, at least in the downward shortwave fluxes. Many of the cases found in the *Wecoma's* observations showed temporal stability of 1 to 2 h and even longer, suggesting that the clearings had radii that were several tens of kilometers. Under such conditions, aside from instrument noise and any instrument sensitivity to temperature and ventilation changes not accounted for in the data processing, the only variations in the downward fluxes are due to changes in the solar zenith angle for the shortwave flux and changes in humidity, temperature, and aerosol properties, which affect both the shortwave and longwave fluxes. Owing to the relatively cold ocean temperatures in the northeastern Pacific, cloud-free conditions are relatively dry. If, in addition, the region is distant from aerosol sources, the variations in aerosol burdens are likely to be small. The strategy for identifying cloud-free conditions in the shipboard radiometer data was thus to seek periods during which the short-term variability of the downward fluxes was relatively

small and any long-term variability was the result of the changing solar zenith angle.

In this study a normalized downward shortwave flux, the downward shortwave flux divided by the cosine of the solar zenith angle, is used instead of the shortwave flux itself. The normalized shortwave flux is a measure of the broadband shortwave transmittance of the atmosphere. The solar zenith angle clearly controls both the magnitude of the shortwave flux and its variability. Dividing the shortwave flux by the cosine of the solar zenith angle removes this first-order influence, leaving the somewhat smaller dependence of the direct and diffuse transmittance on solar zenith angle.

Figure 1 illustrates a somewhat ideal example of cloud-free conditions in the *Wecoma* observations. The figure shows the normalized downward shortwave radiative flux and the downward longwave radiative flux. The 1-min observations (open symbols) are shown along with fluxes calculated using analyzed fields of temperature and humidity at the position of the ship for the 1800 and 2400 UTC analyses bracketing the observations. The sun–earth distance at the time of the observation has been accounted for in the calculations of the normalized downward shortwave flux. In addition, the figure shows the *Terra* CERES CRS constrained

TABLE 1. Downward normalized shortwave fluxes ( $W m^{-2}$ ) obtained with the *Wecoma* and *Thomas G. Thompson* (indicated with <sup>T</sup>) pyranometers and the CERES CRS estimates including constrained CRS, initial CRS, model A, and model B, and the model simulations used to assess the performance of the pyranometers. The values reported for the shipboard data are means and std devs of the 30 one-minute samples centered on the *Terra* overpass. Mean and RMS differences between the CERES FOVs and the shipboard means are given for the CRS products. The simulated values are for a marine aerosol with  $0.55\text{-}\mu m$  optical depth of 0.05 and the mean and RMS differences are for the 30 one-minute shipboard samples.

| Date                     | CERES FOVs | Surface flux |         | Constrained CRS |       | Initial CRS |       | Model A |       | Model B |       | Simulated |       |
|--------------------------|------------|--------------|---------|-----------------|-------|-------------|-------|---------|-------|---------|-------|-----------|-------|
|                          |            | Mean         | Std dev | Mean            | RMS   | Mean        | RMS   | Mean    | RMS   | Mean    | RMS   | Mean      | RMS   |
| 16 May 2001 <sup>T</sup> | 2          | 1064.44      | 3.64    | -5.08           | 8.44  | -9.43       | 12.49 | -6.84   | 9.83  | -6.58   | 9.79  | 6.22      | 6.99  |
| 20 May 2001 <sup>T</sup> | 5          | 1074.96      | 4.40    | -9.46           | 9.51  | -6.77       | 6.84  | -10.85  | 12.10 | -12.46  | 12.78 | -4.11     | 4.69  |
| 21 May 2001 <sup>T</sup> | 8          | 1069.78      | 1.75    | -12.53          | 14.63 | 2.17        | 6.35  | 8.32    | 8.81  | -3.98   | 5.44  | -3.12     | 3.48  |
| 22 May 2001 <sup>T</sup> | 2          | 1079.24      | 3.36    | -15.75          | 15.92 | -5.61       | 6.74  | -6.61   | 6.74  | -17.70  | 17.92 | -6.80     | 6.86  |
| 26 May 2001 <sup>T</sup> | 3          | 1059.94      | 1.98    | -4.05           | 4.62  | -6.87       | 5.94  | —       | —     | -19.66  | 20.38 | 3.22      | 3.08  |
| 30 May 2001 <sup>T</sup> | 18         | 1064.31      | 1.64    | -15.36          | 15.32 | -3.97       | 5.86  | 0.78    | 4.36  | -12.02  | 13.01 | -4.67     | 4.79  |
| 31 May 2001 <sup>T</sup> | 10         | 1064.83      | 7.50    | -10.06          | 12.01 | -14.33      | 15.30 | —       | —     | 15.78   | 16.55 | 1.24      | 0.62  |
| 7 Jun 2001               | 5          | 1028.66      | 5.06    | 14.21           | 18.58 | 16.89       | 19.43 | —       | —     | 15.26   | 16.45 | 18.49     | 19.66 |
| 9 Aug 2001               | 8          | 1049.35      | 2.89    | -6.84           | 7.28  | 3.27        | 3.59  | 1.34    | 3.25  | -4.35   | 5.18  | -3.23     | 3.28  |
| 19 Aug 2001              | 6          | 1052.99      | 2.88    | -10.64          | 10.98 | 2.45        | 3.66  | -5.91   | 6.28  | -9.29   | 10.38 | -2.93     | 2.96  |
| 20 Aug 2001              | 13         | 1044.29      | 1.06    | -10.68          | 11.02 | 3.41        | 3.60  | -11.13  | 11.32 | -16.03  | 16.28 | -6.43     | 6.52  |
| 25 Aug 2001              | 18         | 1058.72      | 3.55    | -15.12          | 16.34 | -12.56      | 14.73 | -15.91  | 15.93 | -19.48  | 19.50 | -6.76     | 6.78  |

estimates for the cloud-free and nearly cloud-free fields of view for ocean scenes within 50 km of the *Wecoma* at the time of the overpass. The results in the figure illustrate the temporal stability of the shipboard measurements under cloud-free conditions.

Figure 1 also shows sensitivities of the calculated fluxes to variations in temperature and humidity profiles and to varying aerosol burdens. The normalized shortwave flux is most sensitive to aerosol burden. Occasionally changes in the moisture burden between 1800 and 2400 UTC have a noticeable impact on the calculated shortwave flux, but in this case, the profiles of temperature and humidity at the two times were rather similar. If the  $0.55\text{-}\mu m$  optical depth were set to 0.05, the agreement between the observed and calculated downward normalized shortwave flux would be within 1% ( $10 W m^{-2}$ ). This aerosol optical depth is nearly identical to the 0.05  $0.5\text{-}\mu m$  optical depth derived by Kaufman et al. (2001) from Aerosol Robotic Network (AERONET; Holben et al. 1998) observations as being representative of the unpolluted, baseline value for the Pacific Ocean.

Aerosol burdens have little effect on the downward longwave radiative flux. Results are shown for an aerosol with  $0.55\text{-}\mu m$  optical depth of 0.8 simply to illustrate the relatively small effects of aerosols. Changes in moisture and temperature, however, often noticeably alter the longwave flux. Nonetheless, as with the shortwave flux, assuming a temperature and humidity profile that falls between those of 1800 and 2400 UTC brings agreement between the calculated and observed downward longwave fluxes to within 1%–2% ( $5 W m^{-2}$ ).

Based on the shipboard data available for this study,

12 days were found in which the temporal stability of the radiometer data indicated cloud-free conditions. Comparisons with the model calculations and with CERES CRS estimates are listed in Table 1 for the downward normalized shortwave flux and in Table 2 for the downward longwave flux. For the downward normalized shortwave flux, the simulated fluxes in which a marine aerosol with  $0.55\text{-}\mu m$  optical depth of 0.05 was assumed are within 2% of the observed fluxes. Interestingly, similar results were found for the “initial” CERES CRS estimates which, while independent of the model simulations performed here, are conceptually the same. While still within 2% of the shipboard observations, somewhat poorer agreement was found for the “constrained” CERES CRS estimates, which tended to underestimate the downward flux at the surface. Presumably, aerosol was added as part of the column adjustments required to achieve agreement between the observed and modeled shortwave radiative fluxes at the top of the atmosphere in the constrained estimates. The CERES parametric models A and B were also within 2% of the shipboard observations, but there was somewhat less agreement than obtained with the simulations performed here.

For the downward longwave fluxes, with the exception of 7 June 2001, the simulated, initial, and constrained CERES CRS estimates were all within 2% of the observed flux. The estimates for 7 June were just worse than 3%. The CERES statistical models were also generally within 2%–3%.

While 12 occasions of temporally stable shipboard fluxes could be found in the available data, the availability of the CERES CRS observations prompted a

TABLE 2. Same as in Table 1 but for the downward longwave fluxes ( $W m^{-2}$ ) obtained with the *Wecoma* and *Thomas G. Thompson* (indicated by  $T$ ) pyrometers.

| Date                     | CERES<br>FOVs | Surface flux |         | Constrained CRS |       | Initial CRS |       | Model A |       | Model B |       | Simulated |       |
|--------------------------|---------------|--------------|---------|-----------------|-------|-------------|-------|---------|-------|---------|-------|-----------|-------|
|                          |               | Mean         | Std dev | Mean            | RMS   | Mean        | RMS   | Mean    | RMS   | Mean    | RMS   | Mean      | RMS   |
| 16 May 2001 <sup>T</sup> | 2             | 292.39       | 3.64    | -2.97           | 4.20  | -3.12       | 6.42  | -3.35   | 8.50  | -3.29   | 8.96  | -0.80     | 1.67  |
| 20 May 2001 <sup>T</sup> | 5             | 305.11       | 4.40    | -2.65           | 3.84  | -4.31       | 4.86  | -1.92   | 2.28  | -0.60   | 2.87  | -3.89     | 4.01  |
| 21 May 2001 <sup>T</sup> | 8             | 325.03       | 1.75    | -1.69           | 6.14  | -5.25       | 7.28  | -7.70   | 8.98  | -7.54   | 8.65  | -2.11     | 2.66  |
| 22 May 2001 <sup>T</sup> | 2             | 329.47       | 3.36    | -5.75           | 6.61  | -1.65       | 3.46  | -5.61   | 6.63  | -6.64   | 7.10  | 1.21      | 1.80  |
| 26 May 2001 <sup>T</sup> | 3             | 303.22       | 1.98    | 4.26            | 6.08  | 3.86        | 4.59  | —       | —     | 9.81    | 10.53 | 3.65      | 3.87  |
| 30 May 2001 <sup>T</sup> | 18            | 320.88       | 1.64    | 2.98            | 5.56  | -3.81       | 5.02  | -7.07   | 7.19  | -8.55   | 8.90  | -0.20     | 0.22  |
| 31 May 2001 <sup>T</sup> | 10            | 325.08       | 7.50    | -2.46           | 6.62  | 4.28        | 6.82  | —       | —     | 8.44    | 8.98  | -5.26     | 4.63  |
| 7 Jun 2001               | 5             | 321.09       | 5.06    | -10.84          | 13.31 | -12.31      | 12.58 | —       | —     | -12.69  | 14.33 | -10.73    | 12.62 |
| 9 Aug 2001               | 8             | 330.02       | 2.89    | 5.76            | 8.87  | 1.08        | 6.12  | 0.26    | 6.23  | -5.07   | 8.45  | 3.62      | 3.66  |
| 19 Aug 2001              | 6             | 311.70       | 2.88    | 3.65            | 5.02  | -1.58       | 3.59  | -6.31   | 7.44  | -3.29   | 5.50  | 0.87      | 0.89  |
| 20 Aug 2001              | 13            | 321.31       | 1.06    | 2.31            | 6.43  | -6.27       | 6.53  | -8.78   | 10.10 | -7.88   | 9.05  | 3.56      | 3.64  |
| 25 Aug 2001              | 18            | 322.20       | 3.55    | -0.97           | 4.75  | -4.46       | 6.62  | -3.97   | 5.34  | -3.33   | 4.89  | -1.71     | 1.72  |

search for cloud-free conditions over the *Wecoma* that may not have been detected on the basis of the temporal stability suggested by the results shown in Fig. 1. Figure 2 shows observations from the *Wecoma* on 4 February 2003. The CERES CRS data indicate 13 fields of view that were cloud free and an additional two fields of view with less than 5% cloud cover within 50 km of the *Wecoma* at the time of the *Terra* overpass. Examination of the *Terra* 1-km MODIS imagery for the location of the *Wecoma* at the time of the overpass suggested that the clouds nearest the ship were part of a low-level layer of broken clouds more than 25 km to the west. If visible from the ship, such clouds would have been just above the horizon. The erratic behavior

of the downward normalized shortwave flux is unexplained.

In all, six such cloud-free cases were found, and in many of these, the pyranometer behaved even more erratically than is shown in Fig. 2. Tables 3 and 4 list the statistics given in Tables 1 and 2 but for the cloud-free days on which the *Wecoma's* pyranometer was erratic. The erratic behavior was limited primarily to the pyranometer. The downward longwave fluxes were somewhat more quiescent and appeared to be largely free of such behavior. Interestingly, four of these cloud-free cases occurred in February 2003. For these cases, the air was cold and water vapor amounts were low, of order  $1.5 g cm^{-2}$  and less. The low water vapor burdens

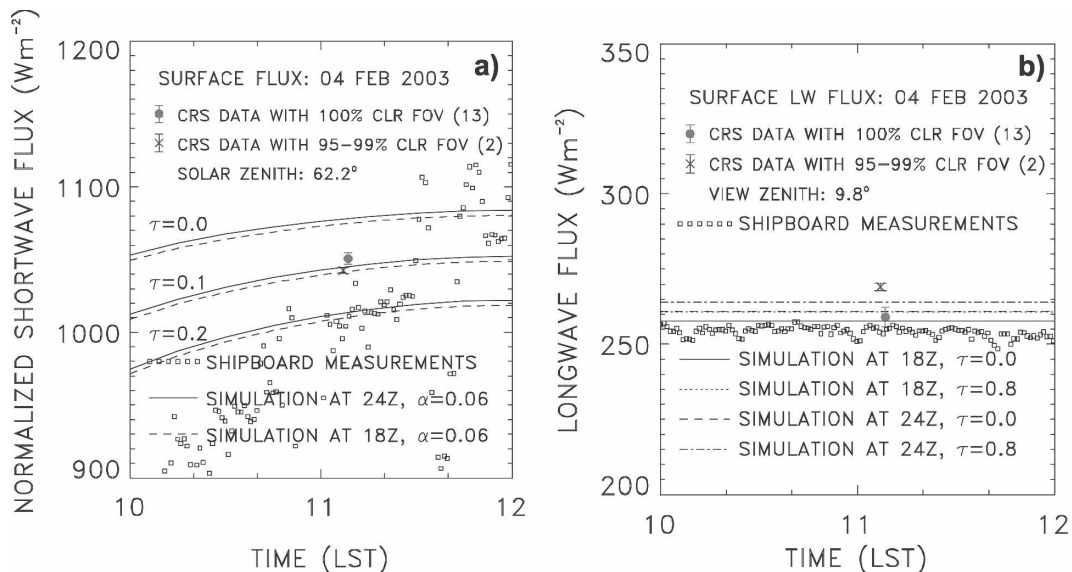


FIG. 2. Same as in Fig. 1, but for 4 Feb 2003. The time was selected on the basis of the cloud-free CERES fields of view found within 50 km of the *Wecoma* location at the time of the *Terra* overpass. The ship was at  $44.2^{\circ}N$ ,  $124.9^{\circ}W$  at the time of the overpass.

TABLE 3. Same as in Table 1, but for days on which the *Wecoma* pyranometer exhibited unexplained erratic behavior.

| Date        | CERES FOVs | Surface flux |         | Constrained CRS |        | Initial CRS |        | Model A |       | Model B |        | Simulated |        |
|-------------|------------|--------------|---------|-----------------|--------|-------------|--------|---------|-------|---------|--------|-----------|--------|
|             |            | Mean         | Std dev | Mean            | RMS    | Mean        | RMS    | Mean    | RMS   | Mean    | RMS    | Mean      | RMS    |
| 2 Jun 2000  | 4          | 1029.78      | 17.07   | 7.55            | 12.13  | 10.93       | 12.17  | —       | —     | 3.30    | 7.12   | 26.72     | 27.14  |
| 14 Jun 2000 | 7          | 1029.15      | 11.15   | -21.73          | 22.18  | -3.83       | 4.80   | 2.55    | 4.26  | 0.21    | 4.10   | 13.43     | 14.88  |
| 4 Feb 2003  | 15         | 975.88       | 62.56   | 63.29           | 63.45  | 55.16       | 55.29  | —       | —     | 57.21   | 57.34  | 70.76     | 73.41  |
| 5 Feb 2003  | 3          | 926.54       | 88.46   | 78.47           | 78.50  | 82.89       | 82.90  | 48.80   | 48.81 | 80.75   | 80.77  | 108.91    | 111.23 |
| 7 Feb 2003  | 8          | 950.42       | 11.81   | 105.83          | 105.89 | 107.68      | 107.74 | 77.54   | 77.71 | 98.07   | 98.13  | 125.12    | 127.01 |
| 8 Feb 2003  | 11         | 703.21       | 349.23  | 337.96          | 337.99 | 332.86      | 332.97 | —       | —     | 333.86  | 333.87 | 352.37    | 358.42 |

coupled with the cold temperatures under cloud-free conditions led to the rather low values of the downward longwave radiative flux measured with the pyrgeometer. The occurrence of the unexpected and unexplained behavior in the pyranometer prompted a search for constraints that would select the shipboard data to be used in assessments of the CERES CRS flux estimates.

**4. Acceptance criteria for shipboard flux measurements**

The erratic behavior of the pyranometer was characterized by rapid variability in the 1-min samples. This variability motivated a search for periods that were temporally stable, at least over relatively short intervals. Temporally stable conditions were sought regardless of the sky conditions, whether cloud-free or cloudy. One-minute samples that have nearly the same values over a period of several minutes are less suspect than those that fluctuate wildly over the same interval. While the fluctuations in the pyranometer data could be valid, for example, they might be caused by sunlight reflected from the sides of clouds or by the sun being blocked by clouds in a broken cloud system, they might also be caused by the buildup of salt on the pyranometer’s filter dome, or by electronic noise that could arise from faulty or corroded connections, or electromagnetic interference, or they could arise from shadows and reflections caused by movements of the ship’s

crane. The strategy was thus to seek periods of observation during which the pyranometer and pyrgeometer outputs were reasonably stable. The temporal variations of the radiometer measurements were examined to determine what might be called “reasonable” variability.

Figure 3 shows means and standard deviations of the downward longwave and normalized shortwave fluxes from a cruise in August 2001. The means and standard deviations were calculated for 30-min periods of the 1-min samples with the starting time of each 30-min period shifted by 15 min. The observations were restricted to solar zenith angles less than 75°. On this cruise, data were collected from 4 to 25 August. There were just over 930 30-min groupings of the 1-min samples that satisfied the solar zenith angle requirement. Results for the month of August 2001 are shown, but results for other months had similar characteristics.

Figure 3a clearly shows 1) the large variability of the downward normalized shortwave radiative fluxes and 2) the range of downward longwave radiative fluxes for August 2001. The extremes of the longwave fluxes were associated with occurrences of temporally stable normalized shortwave radiative fluxes as indicated by the small values of the standard deviations for the 30-min samples. The minimum of the downward longwave radiative flux, centered at approximately 310 W m<sup>-2</sup> and associated with temporally stable normalized shortwave fluxes, with standard deviations less than 10 W m<sup>-2</sup>, characterized cloud-free conditions. Not surpris-

TABLE 4. Same as in Table 2, but for days on which the *Wecoma* pyranometer exhibited erratic behavior. The pyrgeometer seems to have performed normally on these days.

| Date        | CERES FOVs | Surface flux |         | Constrained CRS |       | Initial CRS |       | Model A |       | Model B |       | Simulated |       |
|-------------|------------|--------------|---------|-----------------|-------|-------------|-------|---------|-------|---------|-------|-----------|-------|
|             |            | Mean         | Std dev | Mean            | RMS   | Mean        | RMS   | Mean    | RMS   | Mean    | RMS   | Mean      | RMS   |
| 2 Jun 2000  | 4          | 316.78       | 0.49    | -18.41          | 19.78 | -20.20      | 21.04 | —       | —     | -23.49  | 24.08 | -19.98    | 20.81 |
| 14 Jun 2000 | 7          | 337.25       | 2.75    | 24.56           | 24.67 | 4.30        | 4.43  | -13.44  | 13.49 | -14.99  | 15.07 | -6.40     | 6.48  |
| 4 Feb 2003  | 15         | 254.20       | 1.39    | 6.14            | 7.59  | 5.95        | 6.77  | —       | —     | -0.42   | 4.63  | 3.85      | 3.86  |
| 5 Feb 2003  | 3          | 250.44       | 5.29    | 18.97           | 19.52 | 15.82       | 16.07 | 14.86   | 15.46 | 10.76   | 11.63 | 14.59     | 14.82 |
| 7 Feb 2003  | 8          | 259.08       | 0.53    | 2.04            | 3.15  | -0.08       | 2.13  | -0.56   | 1.85  | -4.89   | 5.69  | -6.58     | 6.65  |
| 8 Feb 2003  | 11         | 255.16       | 6.80    | -1.67           | 3.15  | -3.30       | 4.15  | —       | —     | -3.66   | 3.94  | 8.96      | 9.48  |

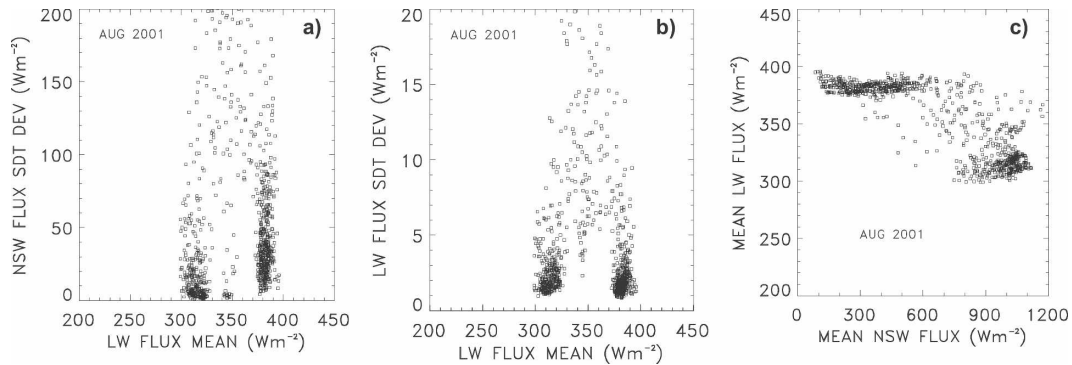


FIG. 3. (a) Average downward longwave flux and standard deviation of downward normalized shortwave flux, (b) average longwave and std dev of longwave flux, and (c) average longwave and normalized shortwave flux. Each point represents the average and std dev of 1-min samples for 30-min periods. The 30-min periods are started every 15 min. The observations are for 4–25 Aug 2001 and for solar zenith angles less than  $75^{\circ}$ . There were just over 930 30-min groups of the 1-min measurements that satisfied the solar zenith angle condition.

ingly, as shown in Fig. 3b, the downward longwave flux also showed remarkable temporal stability under cloud-free conditions—standard deviations less than  $5 W m^{-2}$ . The longwave flux reached a maximum, centered around  $390 W m^{-2}$ , while again showing remarkable temporal stability. At least for some periods when the longwave flux was near its maximum, the normalized shortwave radiative flux also achieved temporal stability, with standard deviations less than  $100 W m^{-2}$ . These conditions probably were associated with skies overcast by low-level clouds. The observations with temporally stable longwave and shortwave fluxes, for which the longwave flux was approximately  $340 W m^{-2}$ , were probably associated with extensive cover by midlevel or upper-level cloud systems. The systems were evidently relatively transparent as can be judged by the values of the downward shortwave flux associated with the clustering of observations shown in Fig. 3c.

Results like those shown in Fig. 3 suggested criteria for temporal stability in the shortwave record. Under cloud-free conditions, rather restrictive limits on temporal variation seemed in order. The limits adopted were 1) the standard deviation of the 1-min samples for a 15-min record of longwave flux had to be less than  $5 W m^{-2}$ ; 2) the standard deviation of the 1-min samples for a 15-min record of normalized shortwave flux had to be less than  $10 W m^{-2}$ , and 3) the standard deviation of the 1-min samples for the 30-min record centered on the 15-min record of the normalized shortwave flux also had to be less than  $10 W m^{-2}$ .

Once the criteria for the cloud-free conditions were set, those for the temporal stability of the normalized shortwave radiative flux were relaxed in order to allow observations of cloudy scenes. The prominent signature

in the downward longwave flux associated with low-level clouds suggested that a standard deviation in the normalized shortwave flux of order  $100 W m^{-2}$  could be tolerated when low-level clouds were present. The cutoff in the standard deviations of 1-min samples in 15-min records of the normalized shortwave flux was set to change linearly with the downward longwave flux as it ranged from the 5th percentile of the longwave fluxes associated with cloud-free conditions to the 95th percentile of the longwave fluxes associated with the low-level cloud layer, those with standard deviations of the 1-min samples within 15-min records of the longwave flux less than  $5 W m^{-2}$ . These criteria were established for each month and then applied to all daytime observations within the month having solar zenith angles less than  $75^{\circ}$ .

Figure 4 shows the observations that remained after the criteria were applied. Clearly, episodes in which the normalized shortwave flux varied wildly were removed. Some of these observations may have been valid, but owing to the erratic behavior exhibited by the pyranometer under cloud-free conditions, shown in Fig. 2, periods with large temporal variability in the pyranometer data were suspect. What remained in the temporally stable observations were cloud-free conditions and those associated with what appeared to be fairly uniform cloud cover. As discussed in the next section, of the data available for this study, approximately a quarter was eliminated. Clearly, the fraction eliminated depended on the nature of the conditions observed.

## 5. All-sky comparisons of shipboard and CERES CRS data

Figure 5 shows the downward normalized shortwave and longwave radiative fluxes obtained primarily with



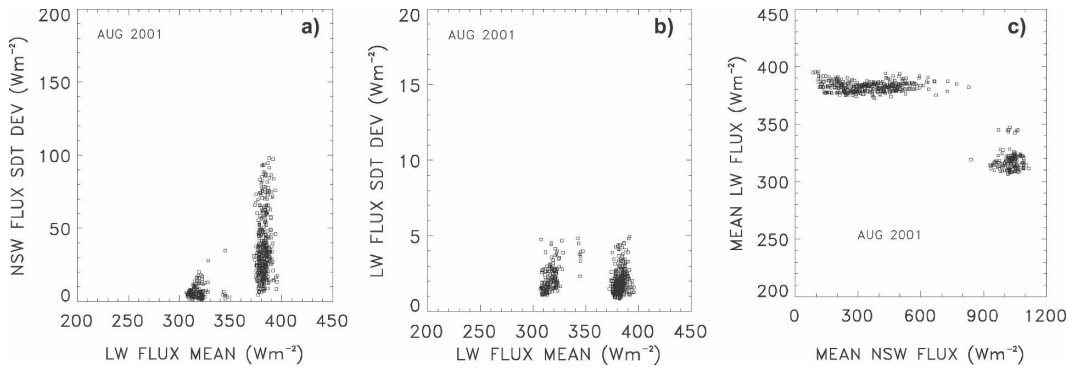


FIG. 4. Same as in Fig. 3, except the observations are those that remain after applying the criteria for temporally stable normalized shortwave fluxes.

the *Wecoma* radiometers and the corresponding CERES CRS constrained estimates. The figure also includes measurements for April–May 2001 obtained with the *Thomas G. Thompson* radiometers. In these comparisons, the mean of the shipboard measurement represents the 30-min average of 1-min samples centered on the time of the *Terra* overpass. The error bars show the standard deviation of 1-min samples. The CERES CRS constrained estimate is the average of the estimates for all fields of view in which the background scene is ocean (i.e., no land) within 50 km of the *Wecoma* at the time of the overpass. The error bars indicate the standard deviation of the fluxes for the selected CERES fields of view.

Of the shipboard observations available for this

study, matchups occurred with the *Terra* CERES observations on 109 days. After applying the criteria to ensure temporally stable shipboard pyranometer data, 81 matchups remained. Table 5 shows the agreement between the downward normalized shortwave radiative flux measured by the shipboard radiometer and the CERES CRS constrained estimate for days on which the *Wecoma* pyranometer exhibited temporal stability at the time of the *Terra* overpass (accepted) and for days on which the pyranometer appeared to behave erratically (rejected). The table includes the average of the solar zenith angles at the times of the overpasses for all of the observations, both accepted and rejected, within the month. Owing to *Terra*'s sun synchronous orbit, within any month there is little difference be-

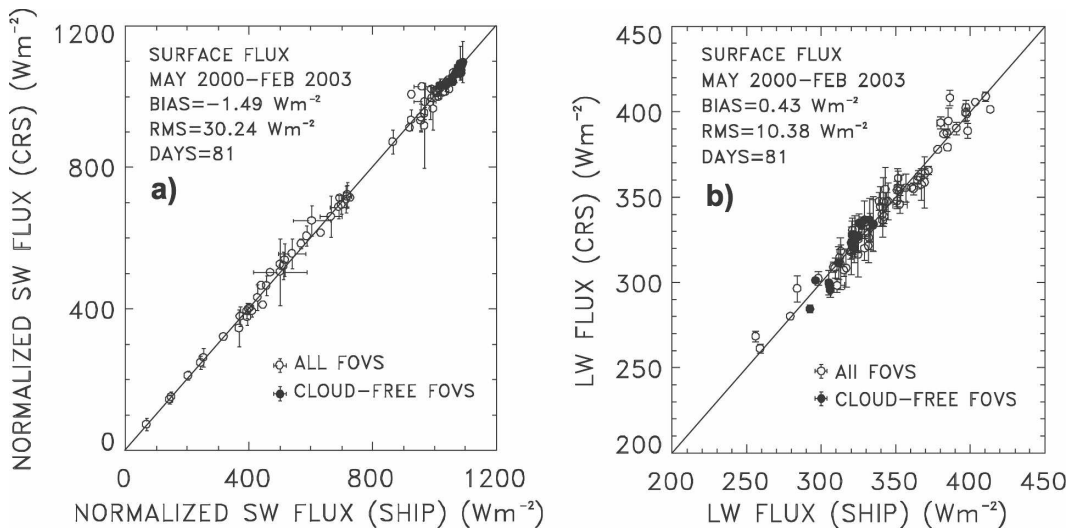


FIG. 5. Downward normalized (a) shortwave and (b) longwave radiative fluxes measured by the shipboard radiometers (SHIP) and estimated by CERES (CRS). Given are the means and the std devs of the 1-min shipboard samples for the 30-min period centered on the *Terra* overpass. The means and standard deviation of the CERES CRS estimates are for all CERES fields of view that were completely over ocean and within 50 km of the ship at the time of the *Terra* overpass.

TABLE 5. Downward normalized shortwave radiative flux ( $\text{W m}^{-2}$ ) measured by the shipboard pyranometer and differences between the CRS constrained estimate and the shipboard observation (CRS-Ship) for days with temporally stable pyranometer behavior (accepted) at the time of the *Terra* overpass and days with erratic pyranometer behavior (rejected). The solar zenith angle is the average of the zenith angles at the times of the satellite overpasses for both accepted and rejected observations. Within a month, there is little difference in the average zenith angle between the accepted and rejected observations.

| Month                                  | Quality of ship data | Days of observations | Mean | Bias  | RMS difference | Solar zenith angle ( $^{\circ}$ ) |
|--|----------------------|----------------------|------|-------|----------------|-----------------------------------|
| <i>Wecoma observations</i>             |                      |                      |      |       |                |                                   |
| May–Jun 2000                           | Accepted             | 13                   | 856  | –12.5 | 35.3           | 22.4                              |
|  | Rejected             | 7                    | 787  | –13.0 | 49.7           |                                   |
| Jul–Aug 2000                           | Accepted             | 5                    | 717  | 4.1   | 28.0           | 28.1                              |
|  | Rejected             | 2                    | 627  | 54.7  | 77.3           |                                   |
| May–Jun 2001                           | Accepted             | 12                   | 911  | 7.2   | 33.3           | 24.0                              |
|  | Rejected             | 8                    | 736  | 8.4   | 44.9           |                                   |
| Aug 2001                               | Accepted             | 18                   | 848  | 0.4   | 20.9           | 34.0                              |
|  | Rejected             | 3                    | 681  | –11.3 | 64.3           |                                   |
| Jan–Feb 2003                           | Accepted             | 15                   | 492  | 4.6   | 28.0           | 64.7                              |
|  | Rejected             | 5                    | 911  | 33.4  | 50.0           |                                   |
| <i>Thomas G. Thompson observations</i> |                      |                      |      |       |                |                                   |
| Apr–May 2001                           | Accepted             | 18                   | 1012 | –10.4 | 37.4           | 25.4                              |
|  | Rejected             | 3                    | 652  | 11.3  | 44.2           |                                   |

tween the solar zenith angles for the accepted and rejected observations. Table 6 provides a similar summary for the downward longwave radiative fluxes. As with the results in Fig. 5, Tables 5 and 6 include results for the *Thomas G. Thompson* radiometers for April–May 2001. Based on the values of the radiative fluxes, the criteria used to select temporal stability generally, but not always, favored conditions with less cloud cover. The observations for January–February 2003 were the exception. In those months, the pyranometer was erratic on what appeared to be mostly cloud-free days.

The results in Tables 5 and 6 illustrate the impact of selecting for skies that produce temporally stable sur-

face radiative fluxes. Because errors that arise from temporal and spatial mismatches were reduced for the observations exhibiting temporal stability, the mean and RMS differences between the CERES CRS estimate and the shipboard measurements both became smaller. Rapid fluctuations in the fluxes, for both the CERES CRS estimates and the shipboard observations, are likely to lead to unrepresentative, and possibly biased estimates of the instantaneous fluxes.

For the observations examined in this study, the agreement between the CERES CRS constrained estimate and the shipboard measurements of the downward normalized shortwave radiative flux within the various months were on average within 2% with an

TABLE 6. Same as in Table 5, but for downward longwave radiative fluxes.

| Month                                  | Quality of ship data | Days of observations | Mean | Bias | RMS difference |
|--|----------------------|----------------------|------|------|----------------|
| <i>Wecoma observations</i>             |                      |                      |      |      |                |
| May–Jun 2000                           | Accepted             | 13                   | 347  | –4.1 | 12.1           |
|  | Rejected             | 7                    | 343  | –7.8 | 13.9           |
| Jul–Aug 2000                           | Accepted             | 5                    | 377  | –1.2 | 8.8            |
|  | Rejected             | 2                    | 398  | 2.5  | 15.7           |
| May–Jun 2001                           | Accepted             | 12                   | 334  | –6.1 | 12.2           |
|  | Rejected             | 8                    | 336  | 7.6  | 15.8           |
| Aug 2001                               | Accepted             | 18                   | 344  | 2.9  | 9.1            |
|  | Rejected             | 3                    | 362  | 3.1  | 11.8           |
| Jan–Feb 2003                           | Accepted             | 15                   | 322  | 6.0  | 11.9           |
|  | Rejected             | 5                    | 268  | 7.2  | 12.6           |
| <i>Thomas G. Thompson observations</i> |                      |                      |      |      |                |
| Apr–May 2001                           | Accepted             | 18                   | 319  | 0.9  | 8.5            |
|  | Rejected             | 3                    | 339  | –6.2 | 10.1           |

RMS difference less than 6% when the criteria for temporal stability were applied. For the days on which the shipboard pyranometer exhibited erratic behavior, the mean difference was as large as 9% and the RMS difference as large as 13% within a given month. For the longwave observations, the agreement between the CERES CRS constrained estimate and the shipboard measurements were largely unaffected by the behavior of the pyranometer. Mean differences were typically less than 2% and RMS differences typically less than 5%. These results are close to those reported by Gupta et al. (2004) who compared the CERES CRS model B estimates with land-based surface measurements. They found that the CERES model B shortwave flux estimates were within 3% of the surface measurements with an RMS difference of 13%. The bias is close to the 2% found for the temporally stable shortwave fluxes while the RMS difference is close to that obtained with no constraints applied to the temporal stability for the shipboard measurements. As noted earlier, temporal stability in the surface measurements are likely to produce observations that are more representative of the sky conditions. Under such conditions, the associated space-based inferences are also likely to produce estimates that are more representative. Consequently, errors due to mismatches in the spatial scales and timing of the observations are reduced, thereby potentially improving the agreement. For the longwave fluxes, Gupta et al. (2004) reported estimates obtained with the CERES CRS model B to be within 1% of the surface measurements with RMS differences of 6% close to the 2% and 5% reported here.

## 6. Conclusions

As has been done by others (Fairall et al. 1998; Medovaya et al. 2002), shipboard measurements of the surface shortwave and longwave radiative fluxes collected off the coast of Oregon were assessed through comparison with calculated fluxes for cloud-free conditions. The cloud-free conditions were first determined on the basis of the shipboard measurements alone. Cloud-free conditions were identified by the temporal stability exhibited by the downward fluxes for periods of at least an hour and, on some occasions, lasting several hours. Aside from its sensitivity to the slowly varying solar zenith angle, the cloud-free downward shortwave flux was rather sensitive to aerosol loading. The cloud-free longwave flux was most sensitive to atmospheric temperature and humidity. Fortunately, off the Oregon coast, owing to the low temperatures of the ocean water and the distances from aerosol sources, the atmosphere is relatively dry and the aerosol burdens light. Initially,

based on the shipboard measurements, *Terra* overpasses occurred with the ship under cloud-free conditions for 12 of the 109 days on which *Terra* CERES data were available and collocated with shipboard measurements. The *Terra* overpasses typically occurred within 1 h of 1100 LT. With the assumption of a marine aerosol with a  $0.55\text{-}\mu\text{m}$  optical depth of 0.05 and using NCEP fields for temperature and moisture, calculated and observed downward shortwave radiative fluxes agreed to within 2%. Likewise, the calculated and observed downward longwave radiative fluxes agreed to within 3%. These accuracies rival the 2%–3% expected of shipboard radiometers (Hosom et al. 1995; Fairall et al. 1998). Consequently, the shipboard observations were presumed sufficiently accurate to assess the performance of the CERES CRS estimates of the surface radiative fluxes. For these cloud-free cases, the CERES estimates were within 2%–3% for both the downward shortwave and longwave fluxes, but a tendency was detected for the CERES “constrained” estimate of the shortwave flux to fall below the shipboard measurements. In the “constrained” estimate, adjustments are made primarily to aerosol and water vapor burdens to achieve the best agreements between calculated and observed shortwave and longwave fluxes at the top of the atmosphere.

In checking the results for the cloud-free comparisons, however, six additional cloud-free overpasses were identified through the analysis of the 1-km satellite imagery that accompanies the CERES CRS estimates. On these overpasses, the 1-min samples of the downward shortwave radiative flux measured by the shipboard pyranometer fluctuated wildly and varied by unacceptable amounts within the 15- and 30-min intervals bracketing the overpass. The rapid fluctuations in the pyranometer data were initially taken to be due to cloudy conditions. Such variability, however, could not be explained by the cloud-free conditions and aerosol burdens derived from the imagery data. While several causes for the erratic behavior are plausible, no specific causes could be found for each of the missed overpasses. Consequently, the erratic behavior of the pyranometer seemed unpredictable and methods were developed to screen the shipboard pyranometer data to avoid cases in which the data might not be valid.

The screening applied to the shipboard observations identified periods that exhibited temporal stability subject to the sky conditions being observed. For cloud-free conditions, the standard deviation of the 1-min samples for the downward normalized shortwave flux within both 15- and 30-min periods had to be less than  $10\text{ W m}^{-2}$ . The 30-min criterion was dropped for cloudy skies and the standard deviation of the 1-min samples

for the downward normalized shortwave flux within 15-min periods was allowed to grow from  $10 \text{ W m}^{-2}$  as a function of the departure of the associated longwave flux from a value near its minimum for the month, its cloud-free value, to  $100 \text{ W m}^{-2}$  when the associated longwave flux was near its maximum, its value for skies overcast by low-level clouds. Cloud-free skies and skies overcast by low-level clouds were readily identified in the downward longwave observations, as the two sky conditions were near the extrema of the observations within a month and they both yielded small standard deviations in the 1-min samples of less than  $5 \text{ W m}^{-2}$  for 30-min periods.

With these criteria for temporal stability applied, mean differences within any month of collocations between the shipboard measurements and the *Terra* CERES CRS estimates were less than 2% for both the longwave and normalized shortwave radiative fluxes. These comparisons included all shipboard observations within  $\pm 15$  min of the *Terra* overpass, and estimates from all CERES fields of view that were over ocean within 50 km of the ship at the time of the overpass. The RMS differences for the daily matchups within a month were less than 6% for the measured shortwave flux. Without the temporal stability criteria, mean differences within a month suffered, rising to as much as 9% while the RMS differences rose to as much as 13%. In most cases, the conditions for temporal stability favored less cloudy conditions as indicated by smaller downward longwave fluxes and larger downward normalized shortwave fluxes. The longwave fluxes were unaffected by the erratic behavior found in the *Wecoma* pyranometer. The average differences for the downward longwave fluxes were within 2% for each month and the RMS differences of the daily matchups within a month were typically less than 5%.

*Acknowledgments.* We thank the marine technicians, especially Linda Fayler, who maintained the radiometers during the cruises examined here. We thank Jack Barth, Tim Cowles, and Alexander Perlin, Oregon State University, for providing the shipboard radiometer data. The shipboard data were collected as part of the U.S. GLOBEC Northeast Pacific Program jointly funded by the National Science Foundation and the National Oceanic and Atmospheric Administration. We also thank Tom Charlock and Fred Rose, NASA Langley, for help with this project and for making available the Langley version of the Fu–Liou Radiative Transfer Code. The CERES CRS data were obtained from the NASA Langley Atmospheric Science Data Center. This paper was prepared by the authors with support from the CERES Science Team, from NASA

through EOS Grant NNG04GM11G, and from the NOAA–Oregon State University Cooperative Institute for Oceanographic Satellite Studies (CIOSS) under Award NA03NES4400001 from the National Oceanic and Atmospheric Administration, U.S. Department of Commerce. The statements, findings, conclusions, and recommendations are those of the authors and do not necessarily reflect the views of the National Oceanic and Atmospheric Administration or the U.S. Department of Commerce.

#### REFERENCES

- Cess, R. D., M. H. Zhang, Y. Zhou, X. Jing, and V. Dvortsov, 1996: Absorption of solar radiation by clouds: Interpretation of satellite, surface, and aircraft measurements. *J. Geophys. Res.*, **101**, 23 299–23 309.
- , T. Qian, and M. Sun, 2000: Consistency tests applied to the measurement of total, direct, and diffuse shortwave radiation at the surface. *J. Geophys. Res.*, **105**, 24 881–24 885.
- Charlock, T. P., and T. L. Alberta, 1996: The CERES/ARM/GEWEX Experiment (CAGEX) for the retrieval of radiative fluxes with satellite data. *Bull. Amer. Meteor. Soc.*, **77**, 2673–2683.
- , F. G. Rose, D. A. Rutan, L. H. Coleman, T. Caldwell, and S. Zentz, 2005: Global multi-year analysis of Clouds and Earth's Radiant Energy System *Terra* observations and radiative transfer calculations. *Proc. 15th ARM Science Team Meeting*, Daytona Beach, FL, NASA, 8 pp. [Available online at <http://www-cave.larc.nasa.gov/cave/pdfs/Charlock.15ARM05.pdf>.]
- Coakley, J. A., Jr., W. R. Tahnk, A. Jayaraman, P. K. Quinn, C. Devaux, and D. Tanré, 2002: Aerosol optical depths and direct radiative forcing for INDOEX derived from AVHRR: Theory. *J. Geophys. Res.*, **107**, 8009, doi:10.1029/2000JD000182.
- Cronin, M. F., N. A. Bond, C. W. Fairall, and R. A. Weller, 2006: Surface cloud forcing in the east Pacific stratus deck/cold tongue/ITCZ complex. *J. Climate*, **19**, 392–409.
- Fairall, C. W., P. O. G. Persson, E. F. Bradley, R. E. Payne, and S. P. Anderson, 1998: A new look at calibration and use of Eppley precision infrared radiometers. Part I: Theory and application. *J. Atmos. Oceanic Technol.*, **15**, 1229–1242.
- Fu, Q., and K. N. Liou, 1992: On the correlated *k*-distribution method for radiative transfer in nonhomogeneous atmospheres. *J. Atmos. Sci.*, **49**, 2139–2156.
- Gupta, S. K., D. P. Kratz, A. C. Wilber, and L. C. Nguyen, 2004: Validation of parameterized algorithms used to derive TRMM–CERES surface radiative fluxes. *J. Atmos. Oceanic Technol.*, **21**, 742–752.
- Hess, M., P. Koepke, and I. Schult, 1998: Optical properties of aerosols and clouds: The software package OPAC. *Bull. Amer. Meteor. Soc.*, **79**, 831–844.
- Holben, B. N., and Coauthors, 1998: AERONET—A federated instrument network and data archive for aerosol characterization. *Remote Sens. Environ.*, **66**, 1–16.
- Hosom, D. S., R. A. Weller, R. E. Payne, and K. E. Prada, 1995: The IMET (improved meteorology) ship and buoy systems. *J. Atmos. Oceanic Technol.*, **12**, 527–540.
- Ignatov, A., and Coauthors, 2005: Two MODIS aerosol products over ocean on the *Terra* and *Aqua* CERES SSF datasets. *J. Atmos. Sci.*, **62**, 1008–1031.

- Inamdar, A. K., and V. Ramanathan, 1997: On monitoring the atmospheric greenhouse effect from space. *Tellus*, **49B**, 216–230.
- Jing, X., and R. D. Cess, 1998: Comparison of atmospheric clear-sky shortwave radiation models to collocated satellite and surface measurements in Canada. *J. Geophys. Res.*, **103D**, 28 817–28 824.
- Katsaros, K. B., and J. E. DeVault, 1986: On irradiance measurement errors at sea due to tilt of pyranometers. *J. Atmos. Oceanic Technol.*, **3**, 740–745.
- Kaufman, Y. J., A. Smirnov, B. N. Holben, and O. Dubovik, 2001: Baseline maritime aerosol: Methodology to derive the optical thickness and scattering properties. *Geophys. Res. Lett.*, **28**, 3251–3254.
- Kistler, R., and Coauthors, 2001: The NCEP–NCAR 50-Year Reanalysis: Monthly means CD-ROM and documentation. *Bull. Amer. Meteor. Soc.*, **82**, 247–267.
- Li, Z., H. G. Leighton, K. Masuda, and T. Takashima, 1993: Estimation of SW flux absorbed at the surface from TOA reflected flux. *J. Climate*, **6**, 317–330.
- Loeb, N. G., S. Kato, K. Loukachine, and N. Manalo-Smith, 2005: Angular distribution models for top-of-atmosphere radiative flux estimation from the Clouds and the Earth's Radiant Energy System instrument on the *Terra* satellite. Part I: Methodology. *J. Atmos. Oceanic Technol.*, **22**, 338–351.
- MacWhorter, M. A., and R. A. Weller, 1991: Error in measurements of incoming shortwave radiation made from ships and buoys. *J. Atmos. Oceanic Technol.*, **8**, 108–117.
- Medovaya, M., D. E. Waliser, R. A. Weller, and M. J. McPhaden, 2002: Assessing ocean buoy shortwave observations using clear-sky model calculations. *J. Geophys. Res.*, **107**, 3014, doi:10.1029/2000JC000558.
- Minnis, P., D. F. Young, S. Sun-Mack, P. W. Heck, D. R. Doelling, and Q. Trepte, 2003: CERES cloud property retrievals from imagers on TRMM, Terra, and Aqua. *Proc. SPIE 10th Int. Symp. on Remote Sensing: Conf. on Remote Sensing of Clouds and the Atmosphere VII*, Barcelona, Spain, International Society for Optical Engineering, 37–48.
- Remer, L. A., and Coauthors, 2005: The MODIS aerosol algorithm, products, and validation. *J. Atmos. Sci.*, **62**, 947–973.
- Rose, F. G., and T. P. Charlock, 2002: New Fu–Liou code tested with ARM Raman lidar aerosols and CERES in pre-CALIPSO sensitivity study. Preprints, *11th Conf. on Atmospheric Radiation*, Ogden, UT, Amer. Meteor. Soc., P4.8.
- Stamnes, K., S.-C. Tsay, W. Wiscombe, and K. Jayaweera, 1988: Numerically stable algorithm for discrete-ordinate-method radiative transfer in multiple scattering and emitting layered media. *Appl. Opt.*, **27**, 2502–2509.
- Wielicki, B. A., B. R. Barkstrom, E. F. Harrison, R. B. Lee III, G. L. Smith, and J. E. Cooper, 1996: Clouds and the Earth's Radiant Energy System (CERES): An Earth Observing System experiment. *Bull. Amer. Meteor. Soc.*, **77**, 853–868.
- Zender, C. S., B. Bush, S. K. Pope, A. Bucholtz, W. D. Collins, J. T. Kiehl, F. P. J. Valero, and J. Vitko Jr., 1997: Atmospheric absorption during the Atmospheric Radiation Measurement (ARM) Enhanced Shortwave Experiment (ARESE). *J. Geophys. Res.*, **102D**, 29 901–29 916.
- Zhang, Y. C., W. B. Rossow, and A. A. Lacis, 1995: Calculation of surface and top of atmosphere radiative fluxes from physical quantities based on ISCCP data sets. 1. Method and sensitivity to input data uncertainties. *J. Geophys. Res.*, **100**, 1149–1166.